Annals of Botany **127**: 765–774, 2021
doi: 10.1093/aob/mcab017, available online at www.academic.oup.com/aob

ANNALS OF BOTANY
Founded 1887

A water drop-shaped slingshot in plants: geometry and mechanics in the explosive seed dispersal of *Orixa japonica* (Rutaceae)

Lan-Jie Huang[1,*] and Wen-Long Fu[2,3]

[1]*College of Life Sciences, Hubei University, Wuhan 430062, China,* [2]*Key Laboratory of Aquatic Botany and Watershed Ecology, Wuhan Botanical Garden, Chinese Academy of Sciences, Wuhan 430074, China and* [3]*University of Chinese Academy of Sciences, Beijing 100049, China*
** For correspondence. E-mail hnrryeuler@whu.edu.cn*

Received: 9 December 2020 Returned for revision: 28 January 2021 Editorial decision: 4 February 2021 Accepted: 5 February 2021
Electronically published: 20 February 2021

• **Background and Aims** In angiosperms, many species disperse their seeds autonomously by rapid movement of the pericarp. The fruits of these species often have long rod- or long plate-shaped pericarps, which are suitable for ejecting seeds during fruit dehiscence by bending or coiling. However, here we show that fruit with a completely different shape can also rely on pericarp movement to disperse seeds explosively, as in *Orixa japonica*.
• **Methods** Fruit morphology was observed by hard tissue sectioning, scanning electron microscopy and micro-computed tomography, and the seed dispersal process was analysed using a high-speed camera. Comparisons were made of the geometric characteristics of pericarps before and after fruit dehiscence, and the mechanical process of pericarp movement was simulated with the aid of the finite element model.
• **Key Results** During fruit dehydration, the water drop-shaped endocarp of *O. japonica* with sandwich structure produced two-way bending deformation and cracking, and its width increased more than three-fold before opening. Meanwhile the same shaped exocarp with uniform structure could only produce small passive deformation under relatively large external forces. The endocarp forced the exocarp to open by hygroscopic movement before seed launching, and the exocarp provided the acceleration for seed launching through a reaction force.
• **Conclusions** Two layers of water drop-shaped pericarp in *O. japonica* form a structure similar to a slingshot, which launches the seed at high speed during fruit dehiscence. The results suggest that plants with explosive seed dispersal appear to have a wide variety of fruit morphology, and through a combination of different external shapes and internal structures, they are able to move rapidly using many sophisticated mechanisms.

Key words: Explosive seed dispersal, geometry, mechanical simulation, multi-layered structure, plant movement, Rutaceae, *Orixa japonica.*

INTRODUCTION

Seed dispersal is an important reproductive process for angiosperms (Howe and Smallwood, 1982). During seed dispersal, fruit dehiscence is a common movement, which is always driven by slow water transport within the pericarp (Dumais and Forterre, 2012; Forterre, 2013; Elbaum and Abraham, 2014). Apart from allowing export of seeds from the maternal plant, this movement also provides energy for explosive seed dispersal, which aids in long-distance travel, up to tens of metres from the parent plant (Swaine and Beer, 1977; Sakes *et al.*, 2016; Galstyan and Hay, 2018).

The internal structure and external shape of the pericarp influence the process of fruit dehiscence, and thereby affect the pattern of seed dispersal (Endo *et al.*, 2010; Bar-On *et al.*, 2014), and a variety of delicate structures in the pericarp are often involved (Elbaum and Abraham, 2014; Hofhuis and Hay, 2017; Galstyan and Hay, 2018). In some cruciferous fruits, the pericarp has a layer of asymmetrically thickened epidermal cells, and is composed of many living cells that can actively transport water (Hofhuis *et al.*, 2016). These fruits regulate turgor to open their pericarp during ripening for seed ejection. By contrast, fruits of some species of Geraniaceae and Leguminosae dehisce explosively by hygroscopic (humidity-driven) movement (Van der Burgt, 1997; Evangelista *et al.*, 2011). Their pericarp is composed of many dead cells, which usually form a multi-layered structure and are surrounded by stiff cellulose microfibrils. Although the peels of these fruits have a variety of internal structures, they are very similar in shape, generally being long rods or long plates (Evangelista *et al.*, 2011; Hofhuis *et al.*, 2016; Shtein *et al.*, 2016). These peels drive seed launch directly by releasing stored elastic potential energy by rapid bending or coiling (Witztum and Schulgasser, 1995; Elbaum and Abraham, 2014). However, many fruits that spread seeds autonomously have completely different shapes, and the seed launch mechanisms of these fruits have not been studied in detail.

Orixa japonica (Rutaceae) is a dioecious shrub native to East Asia, known for its various quinoline alkaloids (Funayama *et al.*, 1994). The fruits of *O. japonica* are abundantly grown on the branches of female plants, and consist of one to four fruitlets, having water drop-shapes (Zhang and Hartley, 2008). Each fruitlet contains only one seed. When the fruit ripens in autumn, its pericarp dries and cracks over a few days, and the seed inside

© The Author(s) 2021. Published by Oxford University Press on behalf of the Annals of Botany Company.
All rights reserved. For permissions, please e-mail: journals.permissions@oup.com.

is dispersed explosively (Zhang and Hartley, 2008). The present research aims to show how the pericarps move during seed dispersal of *O. japonica* through study of the fruit structure, pericarp geometric character and seed dispersal process, and through the mechanical simulation of pericarp movement, to investigate the mechanism of seed launch of these strangely shaped fruit.

MATERIALS AND METHODS

Study materials

Fruits of *Orixa japonica* Thunb. were collected from wild plants distributed in the Shengnongjia Forest Region and Dabie Mountains, Hubei Province, China, during September 2017 and 2019. Experiments were carried out from 2017 to 2020.

Morphological observation and geometric measurement

Mature fruitlets were collected from the plants before dehiscence. These fruitlets were scanned using micro-computed tomography (micro-CT) (ZKKS Sharp-I, Guangzhou, China), and a three-dimensional (3-D) model of the fruitlet was digitally constructed based on the CT images using Mimics version 17 (Materialise, Leuven, Belgium). To observe the microstructure of the pericarp, the mature fruitlet was embedded in polyethylene glycol (PEG) of 2000 MW, and longitudinal sections (10 µm thick) were cut on a rotary microtome (Leica SM2500, Bensheim, Gemany). These sections were first observed with an orthogonal polarized light under a polarization microscope (Zeiss Axio lab Pol, Jena, Germany) and then in a bright field under a light microscope (Nikon E100, Tokyo, Japan) after staining with 0.5% toluidine blue (w/v in 0.2 M Na_2HPO_4). The exocarp and endocarp were separated from the mature fruitlet, air dried, coated with OsO_4, and observed by scanning electron microscopy (SEM; Hitachi S-3400N, Tokyo, Japan). After releasing the seed, pericarps were rehydrated in water, and then fully dried in a drying cabinet at 20 °C, in order to observe the effect of water content on their morphology. The shape of pericarps before and after drying was compared.

To quantify deformation of the pericarp during fruit dehiscence, three aspects of their geometric properties before and after dehiscence were measured: size, continuity and surface curvature. With the ventral suture of the fruitlets as the long axis, the lengths, widths and heights of the exocarp and endocarp of 100 fruitlets were measured directly before opening using calipers (Chengliang, Chengdu, China). After the seeds had been released, lengths, widths and heights of these dehiscent pericarps were measured in the same direction as before, and their opening angles were measured using a protractor. To obtain changes in the continuity of the pericarp structure during fruit dehiscence, 30 mature fruitlets were photographed using a digital camera before and after fruit dehiscence, and the total and split lengths of dorsal and ventral sutures of their peels were measured using ImageJ (NIH, Bethesda, MD, USA). The cracking ratio of the dorsal and ventral suture was calculated by dividing the split length by the total length of the peels for each fruitlet. CT scans were carried out using a micro-CT device before and after fruit dehiscence to obtain the precise shapes of the exocarp and endocarp. The 3D surface models of the pericarp before and after opening were digitally reconstructed using Mimics and Catia v5 software (Dassault, Paris, France) based on the micro-CT images. The Gaussian and mean curvature of each area on these pericarp surfaces were calculated and compared.

Movement record and analysis

Dehiscing and seed launching of the fruit were recorded to determine movement of each part. Mature fruitlets were placed vertically on a small soft, horizontal cushion. The pericarp was shown to slowly open to a certain extent before seed launch, and this motion was recorded using a digital camera with micro lens (Fuji XT10, Tokyo, Japan) facing the ventral side of the fruit in time-lapse mode, at one frame every 5 min. The seed launch phase was recorded using a high-speed digital camera (FASTCAM SA3 with a 35-mm f/2.0 lens; Photron, San Diego, CA, USA) at a rate of 10 000 fps in the positive direction and another digital camera (Sony DSC-RX 100 V, Tokyo, Japan) at a rate of 1000 fps in the lateral direction, under a high-powered (300-W) incandescent lamp.

Using high-speed videos of seed launch, the position of the exocarp, endocarp and seed at every time step was measured by digitizing the videos using the MATLAB-based program DLTdv5 (Matlab R2012b, Natick, MA, USA). The displacements of the three units at different times during seed launch were calculated separately. The velocity of the seed and endocarp, the angle between the seed flight direction and fruit stalk axis φ_s, and the angle between the endocarp flight direction and fruit stalk axis φ_p after seed launch were calculated. In addition, the opening angle of the exocarp θ during seed launch was measured at different times based on high-speed videos of seed launch by the ImageJ software, including the critical angle of exocarp opening at the beginning of seed launch θ_0, and the opening angle of exocarp after seed was released θ_f.

Physical measurement and mechanical simulation

Based on previous observations on the seed launch process, we used a simplified mechanical model of the fruit to analyse the seed launching process. In this model, the endocarp pushed the exocarp to open by hygroscopic movement before seed launching; this propulsive force caused the exocarp to bend, which produced a pair of reaction forces on the endocarp, and this reaction force was assumed to be the driving force when the seed left the fruit. Based on these assumptions, the theoretical value of the launching velocity of the seed can be calculated using momentum theory:

$$v_0 = \frac{2pt}{m}\sin(\theta_0/2) = \frac{2f_0t}{m}\cos(\theta_0/2)\sin(\theta_0/2); \quad (1)$$

where v_0 is the launching velocity of the seed; p is the propulsive force of the endocarp on the upper edge of the exocarp; t is the time from seed stalk rupture to seed detachment from the endocarp, which is approximately 0.3 ms based on our high-speed videos; m is the total mass of the endocarp

and seed; θ_0 is the critical opening angle of the exocarp at the beginning of seed launch; and f_0 is the equivalent pulling force on both sides of the exocarp when the opening angle was θ_0, and is a function of the elastic modulus of the exocarp E_e, the opening angle of the exocarp after seed release θ_f, and θ_0.

To compare the results of our model with the velocity of seed launching obtained in the movement analysis, physical parameters m and E_e were measured, and equivalent pulling force f_0 was obtained by a tensile test and two simulation experiments. The peels and seeds of 140 mature fruitlets from ten plants were weighed respectively, on an electronic balance (Shimadzu AUW320, Kyoto, Japan), and peel thicknesses were measured with calipers. To obtain the elastic flexural modulus of the exocarp and endocarp, 5-mm segments along the longitudinal direction of the fruit were cut respectively from the exocarps and endocarps of ten dehiscent fruits, and three-point tests of these segments were carried out in a universal material testing machine (Instron 8841, Norwood, MA, USA).

In the tensile test, exocarps of ten fruitlets that had released seeds from different mature fruits were chosen. Two thin wires were passed through the tips of both sides of the exocarp and were clamped on the universal material testing machine. When the tensile forces on both sides increased from 0 N to the maximum tensile force required to break the exocarp at the base, the ventral shape of the exocarp was recorded using a digital camera. The opening angles of the exocarp corresponding to the different tensile forces were measured using the ImageJ software.

The simulations were based on finite element models (FEMs) calculated with a static structure analysis using ANSYS version 14.5 (ANSYS Inc., Canonsburg, PA, USA). The 3-D reconstructed forms of the surfaces of the opened exocarp were imported into ANSYS to generate exocarp models, which were simplified to a uniform thickness for more effective simulation. The tissue material of the exocarp model was idealized to have an isotropic and linear elastic behaviour with a Young's modulus of $E = 4.7$ GPa (average of the flexural modulus of exocarp measured by our experiments) and a Poisson's ratio of $\mu = 0.49$. In the first simulation, the opening angle of the exocarp in the initial model was set to be the same as the average of the measurement results of the exocarp opening-angle in the tensile test. The tips of the two halves of the exocarp were subjected to two horizontal tensile loads in left and right directions from 0 to 2.1 N (the average value of maximum pulling force that keeps the exocarp from breaking in the tensile test experiment), and then the stress distribution on the exocarp under the different tensile loads was analysed, and the displacements of the two tips of the exocarp in left and right directions were obtained, which were used to calculate the opening angle of the exocarp under the different tensile loads. These results were compared with those of the tensile test experiment. In the second simulation, the opening angle of the exocarp in the initial model was set as equal to the average value of the opening angle of the exocarp after the seed was released, θ_f, in the movement analysis. Both ends of the top of the exocarp were subjected to increasing horizontal tensile loads from 0 N to when the opening angle of the exocarp reached the critical opening angle of the exocarp θ_0 in the movement analysis, at which time the value of critical pulling force f_0 and stress distribution on the exocarp were obtained.

RESULTS

Fruit morphology

Mature follicles of *O. japonica* consisted of one to four fruitlets (Fig. 1A). The uncracked fruit was shaped similar to a water drop, with a beak at the top and a pair of small flat areas at the base (Fig. 1B). The mature fruit contained a single globular black seed surrounded by two layers of pericarp (Fig. 1C, D), which were connected to the seed by a small membranous funiculus in the basal flat areas. The thickness of the brown exocarp varied with position in most areas, but was relatively greater at the base junction of the two halves. There was a clear boundary between the flat areas and other areas of exocarp, as this thickness suddenly decreased in the basal flat areas. The yellow endocarp had a relatively uniform thickness. The exocarp and endocarp were 0.3 ± 0.05 mm (mean ± s.d., $n = 90$) and 0.34 ± 0.02 mm ($n = 100$) thick, respectively.

The two pericarps of *O. japonica* had completely different tissue structures (Fig. 1E–L). There was no obvious hierarchical structure in the exocarp (Fig. 1E, H), and it contained a large amount of vascular tissue which was scattered throughout the parenchyma (Fig. 1E). Ductal cells in the vascular tissue had a large internal lumen although the cell wall was thick (Fig. 1I). The endocarp exhibited a sandwich layered structure, with thin outer and inner layers and a thick middle layer (Fig. 1F, J), which were formed by sclerenchyma cells (Fig. 1F). The inner and outer layers contained a single layer of striped cells, the lateral walls of which were thickened and closely aligned (Fig. 1F, K). Both layers had a laminated structure, but the direction of arrangement of this structure was different between the two (Fig. 1F, J). The middle layer contained multi-layered cells, which merged into a single structure due to full thickening of the cell walls and a small lumen (Fig. 1L). The boundary between these cells was not clearly distinguishable by optical microscopy or SEM (Fig. 1F, J).

The exocarp split slightly at the top and retained its water drop-shape when the seed was released from the fruit, but two tips of the endocarp opened widely into a shape similar to a pair of open arms, and the basal areas of the two halves remained connected in the form of a small pocket (Fig. 1D). The rehydrated exocarp and endocarp both reverted to the same shape as before seed dispersal (Fig. 1M). After fully drying, the exocarp cracked very slightly, while the endocarp opened wider than before rehydration (Fig. 1N). This indicated that the endocarp opened automatically through hygroscopic movement during fruit dehiscence, whereas opening of the exocarp was passive.

Geometric properties of the pericarp

Although the shapes of the closed exocarp and endocarp were similar in the three views, the shapes of the opened forms were quite different (Fig. 2A). After the fruit had completely dehisced, the two sides of the exocarp opened at an angle of 32.77 ± 7.34° (mean ± s.d., $n = 100$), whereas the angle of

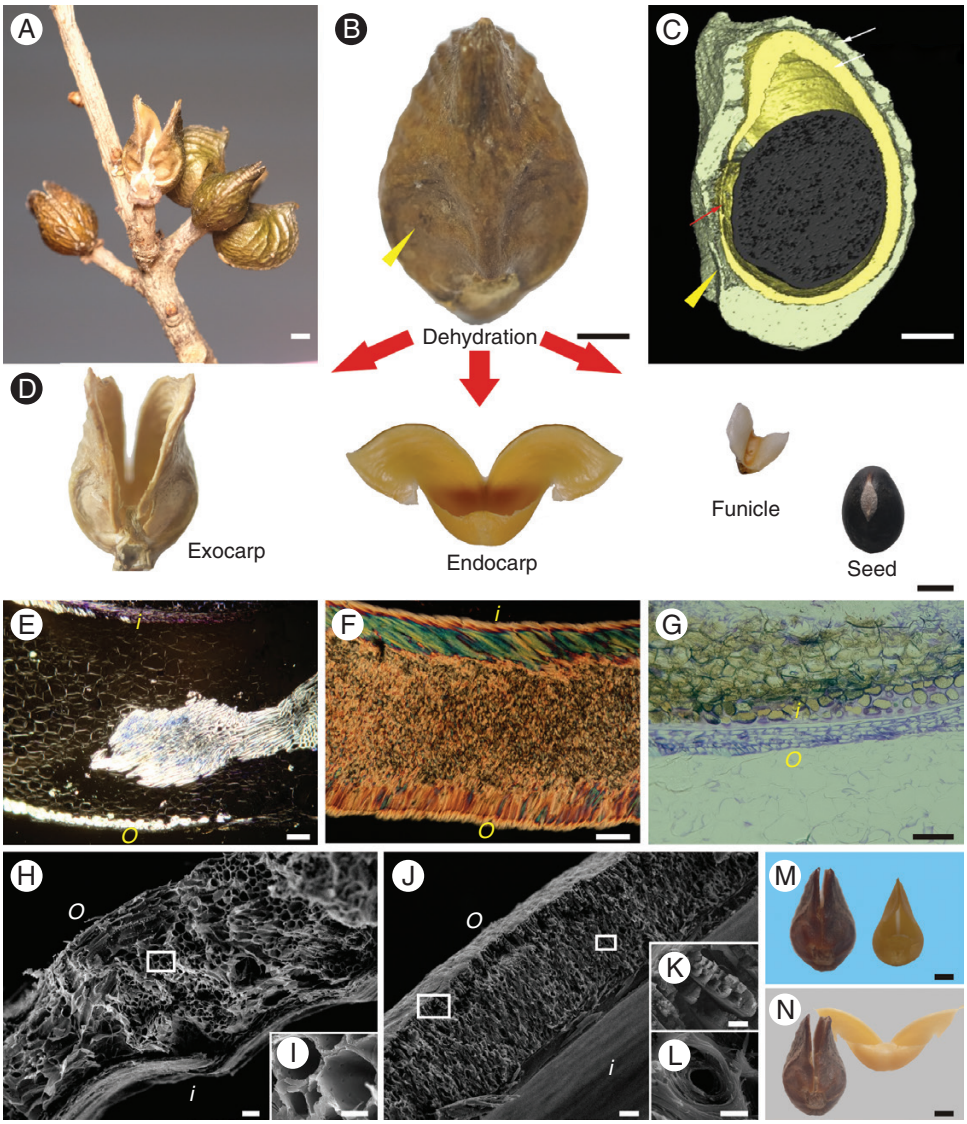

FIG. 1. Fruit morphology of *Orixa japonica*. (A) Mature aggregate of fruits on a wild plant. (B) Lateral view of a fruitlet on the mature fruit. (C) Three-dimensional reconstruction of the fruitlet showing the internal structure obtained by micro-computed tomography. Yellow arrowheads indicate the basal flat area on the pericarp, in which the exocarp becomes very thin. (D) Parts of a fruitlet after seed dispersal. (E) Polarized light micrograph of a transverse section of the exocarp. Bright vascular tissue is scattered in the dark parenchyma. (F) Polarized light micrograph of a transverse section of the endocarp. The endocarp has a sandwich structure composed of two surface layers of nearly parallel cells and multi-layer thick-walled cells in the middle. Different colours in the two surface layers are interference colours caused by different arrangement directions of cell walls. (G) Light micrograph of a transverse section of the testa (brown) and membranous funiculus (violet) stained with 0.5% toluidine blue. (H) Scanning electron micrograph of a cross-section of the exocarp. (I) Magnification of the boxed area in H. (J) Scanning electron micrograph of a cross-section of the endocarp. (K) Magnification of the left boxed area in J. (L) Magnification of the right boxed area in J. (M) Exocarp and endocarp after rehydration. (N) Exocarp and endocarp after being fully dried. o, outside the fruit; i, inside the fruit. Scale bars: A, B, C, D, M and N = 1 mm; E, F, G, H and J = 50 μm; I, K and L = 10 μm.

endocarp reached 102.38 ± 5.88° (n = 100). As shown in Table 1, the length and width of the exocarp increased slightly after opening ($P < 0.01$), but there was no significant change in height ($P > 0.05$). In contrast, endocarp length and height decreased significantly after opening ($P < 0.01$), whereas the width increased more than three-fold prior to opening ($P < 0.01$).

The continuity of the pericarps clearly changed before and after fruit dehiscence. Before dehiscence, the exocarp surface was completely closed. After dehiscence, the exocarp surface was completely broken in the dorsal suture area. Fracture ratios of the ventral suture and the boundary line of the basal flat area were 0.51 ± 0.03 and 0.65 ± 0.08 (mean ± s.d., n = 60), respectively (Fig. 2B). Closed endocarp and ventral membranous funiculus together constituted a closed structure. The dorsal suture on the endocarp surface was broken (~67.6 ± 3.2 %, mean ± s.d., n = 60) after the fruit had cracked (Fig. 2B).

Curvature analysis of the reconstructed surface of the pericarp showed that the distribution of curvature of the exocarp and endocarp surfaces was similar before dehiscence, but quite different after dehiscence (Fig. 2C). The Gauss curvature on the closed exocarp surface was positive at the base and negative at the top, but after the fruit had dehisced, the positive curvature

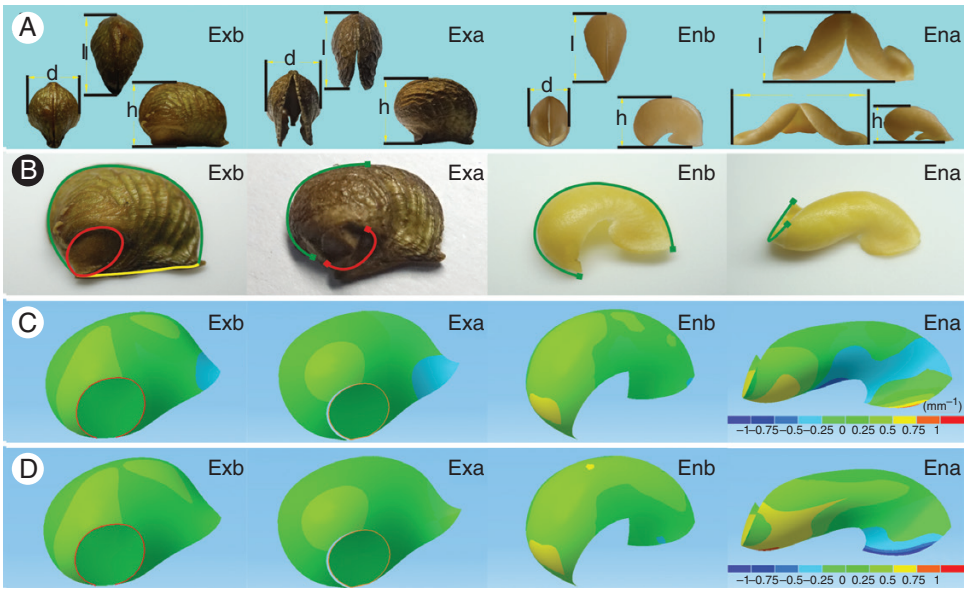

FIG. 2. Geometric properties of the pericarp of *Orixa japonica*. (A) Three-view images of the pericarp before and after fruit dehiscence under the stereomicroscope: l, d and h correspond to the length, width and height of the pericarp, respectively. (B) Continuity of pericarp surfaces before and after fruit dehiscence. The pericarp images were obtained using a stereomicroscope. Green, yellow and red curves represent continuous dorsal suture, ventral suture and boundary line of the jointing area, respectively. (C) Gauss curvature distribution of pericarp surfaces obtained by Mimics and Catia v5 software. The lower right ruler indicates the range of curvature values corresponding to different colours on the surface of the pericarp. (D) Mean curvature distribution of pericarp surfaces obtained by Mimics and Catia v5 software. Ena, dry endocarp after fruit dehiscence; Enb, wet endocarp before fruit dehiscence; Exa, dry exocarp after fruit dehiscence; Exb, wet exocarp before fruit dehiscence.

TABLE 1. *Geometrical parameters of the pericarp before and after fruit dehiscence in* Orixa japonica.

	Exocarp (n = 100)			Endocarp (n = 100)		
	Length (mm)	Width (mm)	Height (mm)	Length (mm)	Width (mm)	Height (mm)
Before dehiscence	8.40 ± 0.67[a]	5.22 ± 0.36[a]	6.31 ± 0.44[a]	7.24 ± 0.30[a]	4.16 ± 0.26[a]	5.10 ± 0.24[a]
After dehiscence	8.53 ± 0.68[b]	5.46 ± 0.43[b]	6.32 ± 0.44[a]	6.01 ± 0.37[b]	13.38 ± 0.69[b]	3.15 ± 0.19[b]

Different superscript letters indicate significant differences before and after dehiscence ($P < 0.05$). Values are presented as mean ± s.d.

region became smaller and the negative curvature region became larger. The Gauss curvature of the closed endocarp surface was also positive at the base and negative at the top, but in contrast to the exocarp, the positive curvature region of the endocarp accounted for a larger proportion and the negative region a smaller proportion. After the fruit was completely dehiscent, the Gauss curvature of the endocarp surface was positive at the top, and negative curvature was only found in the middle. Moreover, the distribution map of mean curvature of the pericarp surface showed that the top and near to the base were the most curved parts of the endocarp, and the bending direction of these two regions was opposite (Fig. 2D).

Kinematics of seed launch

As mature fruits of *O. japonica* dried on the plant, fruitlets dehisced and the seeds were launched from the plant. At the early stage of dehiscence, the two layers of pericarp opened slowly, and opening angles of pericarps gradually increased (Fig. 3A). During this period, the top of the endocarp contacted the top of the exocarp, where it was confined to the exocarp, and the membranous funiculus connecting the seeds was still attached to the endocarp and exocarp. The dorsal and ventral sutures of the exocarp began to split from the top of the fruit, while the exocarp at the boundary of the basal flat area remained intact. After the ventral suture of the exocarp had completely split, the boundary of the basal flat area broke within tens of seconds. When the opening angle of the exocarp increased to 85.35 ± 11.11° (mean ± s.d., n = 30), which was the critical angle for seed launch, θ_0, the membranous funiculus was disconnected from the exocarp, and the endocarp and the seed with membranous funiculus began to exit from the opening at the top of the exocarp (Supplementary Data Video S1).

The endocarp detached from the exocarp after less than 1 ms. During this period, both sides of the endocarp and exocarp were still in contact, but the endocarp and seed continuously slid outward along the top area of the exocarp ventral suture (Fig. 3). After ~0.3 ms, the membranous funiculus broke off from the endocarp, and released the seed from the endocarp. When the endocarp was detached from the exocarp, it was projected at a speed of 5.5 ± 1.1 m s^{-1} (mean ± s.d., n = 35) and the angle between its flight direction and the fruit stalk axis φ_p was 6.31 ± 10.89° (n = 35). At about the same time, the seed projected upward at a speed of 7.8 ± 1.5 m s^{-1} (n = 35) with an angle between its flight direction and fruit stalk axis φ_s of 13.18 ± 9.75° (n = 35)

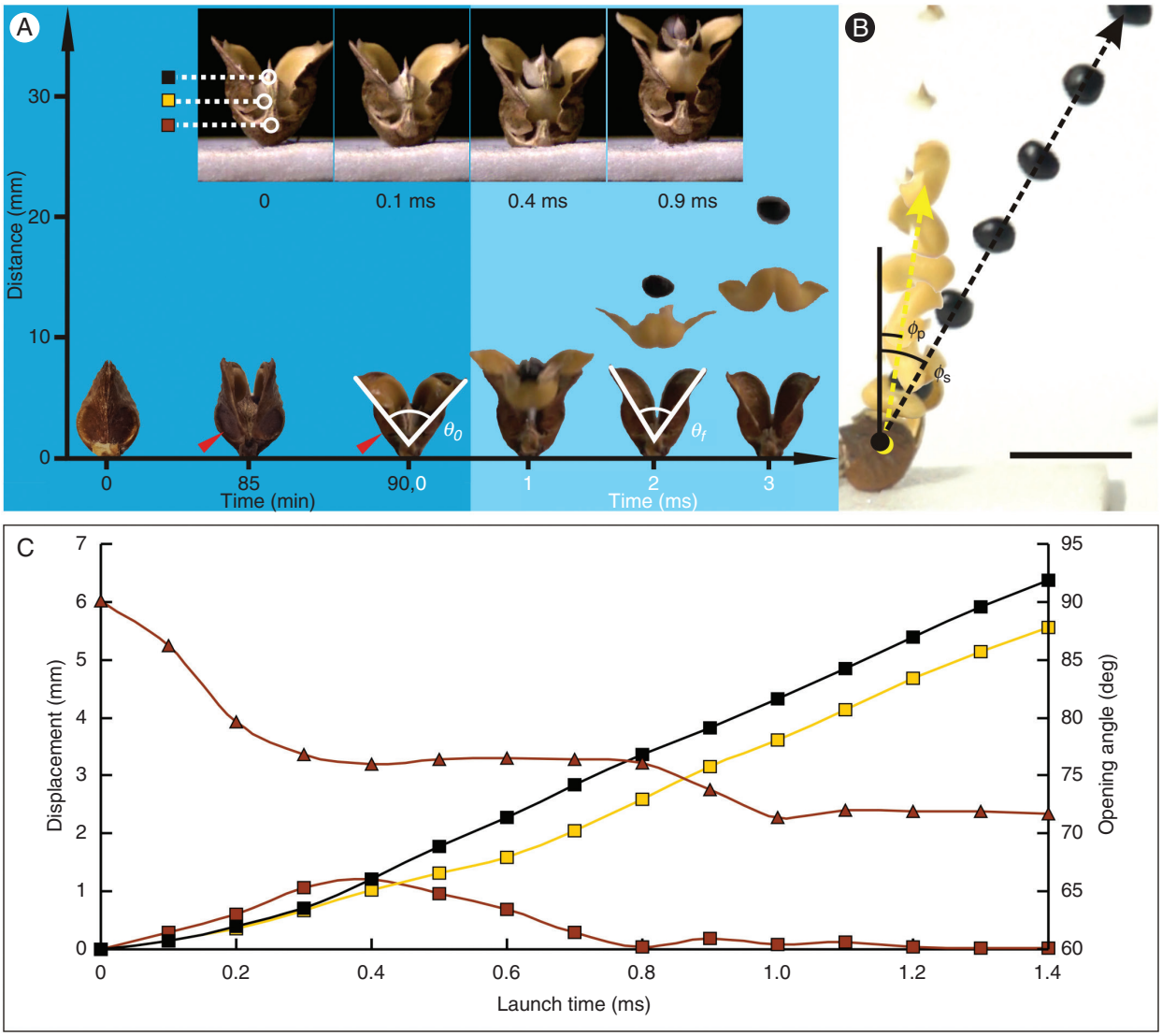

FIG. 3. Seed launching process of *Orixa japonica*. (A) Frontal view of the seed launching process. The horizontal digital axis indicates the time of each state in the seed launching process. The zero time in the dark blue area is when the pericarp begins to crack, and the zero time in the light blue area is when the membranous funiculus in the basal joining area is disconnected from the exocarp. The vertical digital axis indicates the height from the base of the pericarp, θ_0 is the critical angle of exocarp opening at the beginning of seed launch, and θ_f is the opening angle of the exocarp after the seed has left the fruitlet. The red arrow indicates the basal fracture area of the exocarp. The four small inset images show details of endocarp detachment from the exocarp during the first millisecond. The four images show in turn the states of the fruit when the seed is about to be launched, when the funiculus is separated from the exocarp, when the seed is separated from the endocarp, and when the upper arms of the endocarp are separated from the exocarp. In the first small image, three coloured squares indicate different parts of the fruit (black, centre of seed; yellow, ventral base of endocarp; brown, ventral base of exocarp), which are used in C. (B) Composite image of the fruit as the seed is launched by the fruit taken from a 1000-fps video in side direction with 1-cm bar. Each image is 1 ms apart. Yellow and black dotted lines represent flight tracks of the endocarp and seed, respectively, φ_s is the angle between the seed's flight direction and fruit stalk axis, and φ_p is the angle between the endocarp flight direction and fruit stalk axis after seed launch. (C) Changes in opening angle of the exocarp and displacements of three different parts of the fruit during seed launching. The triangles represent opening angles of the exocarp during seed launching; the coloured squares represent the displacements of different parts of the fruit indicated in A. Scale bar = 10 mm.

(Fig. 3B; Supplementary Data Video S2). When the seed and endocarp left the fruitlet, the opening angle of the exocarp, θ_f, became $68.79 \pm 9.79°$ ($n = 30$), which was $16.56 \pm 5.28°$ less than the critical angle for seed launch, θ_0.

In the dynamic curve diagram of seed launch (Fig. 3C), the opening angle of the exocarp decreased with time, while the upward displacement of the endocarp base and seed increased gradually. The downward displacement of the exocarp on the cushion first increased due to recoil motion, and then decreased. The time of maximum displacement correlated with the time when the opening angle of the exocarp reached the minimum stable value during the seed launching process, which also corresponded to the time at which the seed separated from the endocarp. According to slope variations of movement curves of the seed and endocarp, the seed accelerated along with the endocarp before the seed detached from the endocarp. After the seed detached from the endocarp, the upward velocity of the endocarp was clearly less than that of the seed.

Mechanical process of seed launch

Although the dried exocarp of *O. japonica* was not a strictly elastic structure, its opening process was fitted to Hooke's law. In the tensile test, the opening angle of the dried exocarp increased linearly as the tensile force applied on both sides increased (Fig. 4A). When the tensile force increased to 2.09 ± 0.38 N (mean ± s.d., $n = 10$), the basal junction of the exocarp was broken and the two halves separated. The mechanical behaviour of the ideal exocarp model in the FEM simulation was similar to that of the live plant. The physical parameters given in Table 2 were used in the FEM simulation. When the tensile loads on both sides of the model were increased, the opening angle of the model also increased linearly (Fig. 4A). The high degree of stress in the exocarp was distributed mainly in the basal joint area of the two halves, and maximum stress was near the end of the dorsal crack, which was the initial fracture area of the pericarp opening in the tensile test. When the tensile load at both tips of the model reached 2 N, the maximum stress inside the exocarp was ~428 MPa.

The equivalent pulling force exerted by the endocarp on exocarp during seed launch, f_0, was obtained in the second FEM simulation. The initial opening angle of the exocarp model matched the opening angle after the seed was released. When the tensile load applied to both sides was ~1.4 N, the exocarp model opened to the maximum extent of the pericarp opening in the actual seed-dispersal process, confirming that the opening angle of the model was equal to the critical opening angle for seed launch, θ_0, and the maximum stress value in the model was less than that of the first simulation experiment (Fig. 4B).

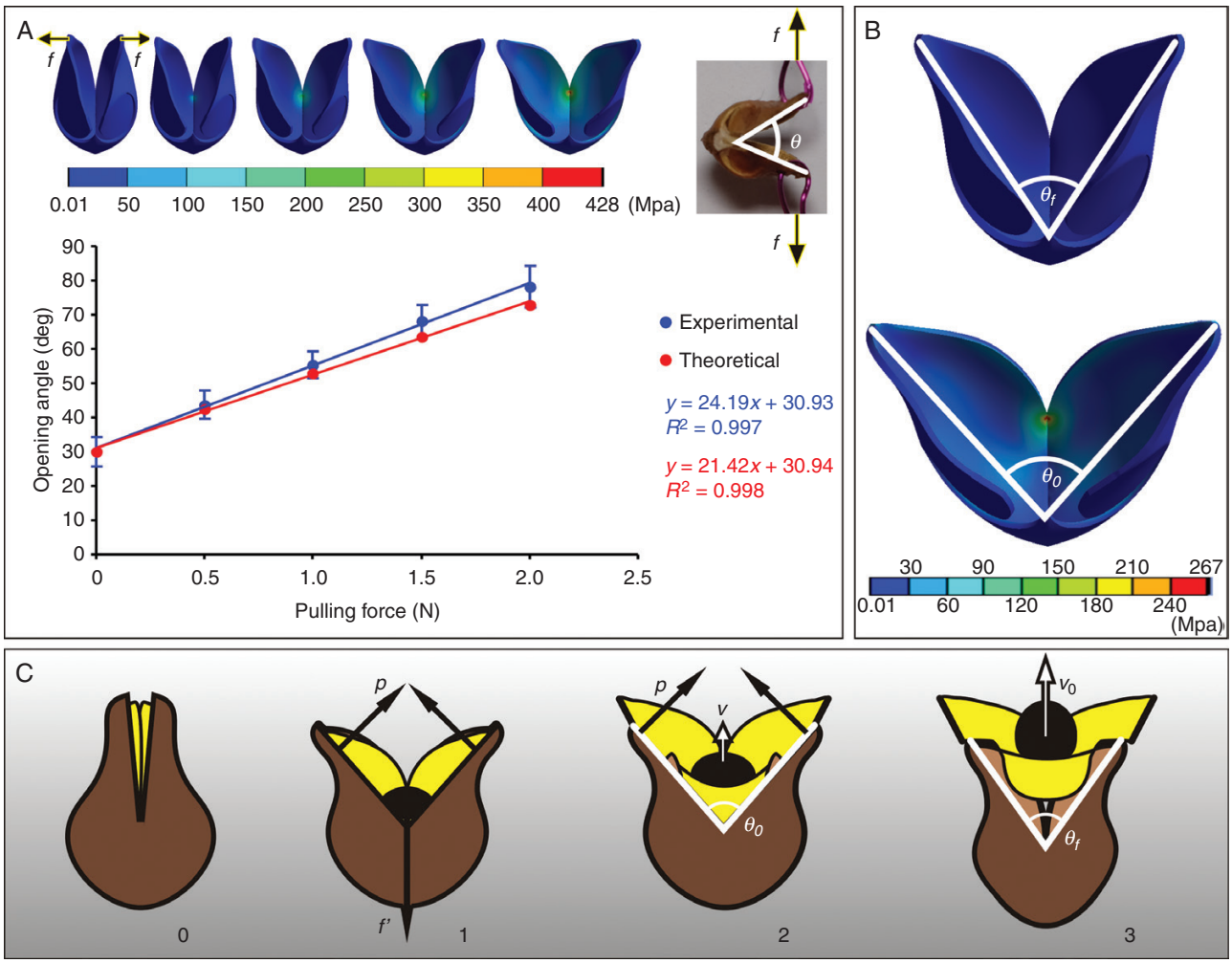

FIG. 4. Biomechanical analysis of pericarp movement during explosive seed dispersal in *Orixa japonica*. (A) Opening angles of the exocarp under different pulling forces in the tensile test are compared to theoretically predicted values in the finite-element model (FEM) simulation. The red and blue lines are the linear fitting curves of experimental and theoretical data respectively, and the fitting equations and R^2 values are displayed on the right-hand side. Error bars of the blue points show the standard deviation of the experimental data. The upper left inset shows the variation of the equivalent stress distribution on the FEM of the exocarp as the tensile load on both sides of the exocarp increases in the simulation, and the upper right insert shows the opening state of the exocarp under pulling force f in the tensile test. (B) Changes of exocarp state and equivalent stress distribution on the exocarp with an opening angle from θ_f to θ_0 in the FEM simulation of exocarp opening. (C) Cartoons of the mechanism of seed launch showing the effect of the interaction between the endocarp (yellow) and the exocarp (brown) on seed (black) acceleration. The numerical sequence below indicates the change of fruit state during seed launching. p, the propulsive force exerted by both sides of the exocarp on the endocarp; f', the tension exerted by the base of the exocarp on the base of the endocarp before the membranous funiculus breaks from the exocarp; v, the velocity of seed movement; v_0, the velocity of seed movement when it leaves the endocarp; θ_0, the critical angle of exocarp opening at the beginning of seed launch; θ_f, the opening angle of the exocarp after seed leaves the fruitlet.

TABLE 2. *Physical parameters of fruit components in* Orixa japonica.

	Mass (mg)	Flexural modulus (GPa)
Exocarp	26.2 ± 4.8***	4.7 ± 1.1***
Endocarp	23.6 ± 3.5***	19.9 ± 13.6**
Seed	27.0 ± 5.6***	

Values are presented as mean ± s.d. ***$P < 0.001$, **$P < 0.01$.

The equivalent pulling force, f_0, was approximately equal to the tensile load of 1.4 N that caused the exocarp model to open to the critical angle for seed launch, θ_0, in the second simulation experiment. Using the value of the equivalent pulling force f_0 (1.4 N), average mass of seeds (27 mg), average mass of endocarps (23.6 mg) and time elapsed by the acceleration of seeds (0.3 ms) into eqn (1), the theoretical initial launching velocity of seeds was ~8.3 m s^{-1}. There was no significant difference between this theoretical value and the experimental values of the initial velocity of seed launching obtained in movement analysis ($P > 0.05$). This result led us to accept the hypothesis that the reaction force of the propulsive force of the endocarp on the upper edge of the exocarp was the driving force for seed launch (Fig. 4C).

DISCUSSION

Many species of angiosperms have the ability to disperse seeds independently (Stamp and Lucas, 1983; Sakes *et al.*, 2016; Galstyan and Hay, 2018). The majority of these launch their seeds by explosive cracking of the pericarp, which is generally a multi-layer composite structure (Galstyan and Hay, 2018). The fruits of *O. japonica* also have a multi-layered pericarp, but unlike the fruits previously studied, the exocarp and endocarp of *O. japonica* are separated from each other rather than fused. The exocarp of *O. japonica* is mainly composed of parenchyma and vascular tissues, which do not form a distinct stratified structure, and the large amount of vascular tissue makes the exocarp stiff. The endocarp of *O. japonica* has a typical composite sandwich structure consisting of a porous interior between two plate-type parts, which consist of a layer of cells with thick cell walls arranged tightly, but the direction of cell-wall arrangement in the two sheets is different. Similar plate-type structures have been found in the pericarp of some legumes (Zohary, 1955). In most cases, the sandwich structures have minimal compliance and weight (Chen *et al.*, 2012); therefore, although the endocarp mass of *O. japonica* is smaller, it has a much higher elastic modulus than an exocarp of similar thickness.

The difference between the exocarp and endocarp of *O. japonica* is not only reflected in their internal structure, but also in their external shape. Before fruit dehiscence, the exocarp surface is closed, and the Gauss curvature of most areas of this surface is positive. The exocarp is closed to the water drop-shape, and the convex ovary provides a large internal space for the seed. Although most areas of the surface of uncracked endocarp also have positive Gauss curvatures and the shape is similar to that of the exocarp, the endocarp surface is not closed, having a large opening on the ventral side. These geometric differences between the two layers of pericarp combined with internal structural differences resulted in completely different types of deformation between them during fruit dehiscence.

Although there are many cells within thickened walls in the exocarp of *O. japonica*, these cells are mainly concentrated in the dispersed vascular bundle, which is surrounded by a large amount of parenchyma. Unlike the pericarp of sesame, there is no obvious layered structure as is seen in the mature sesame pods, which can open hygrosopically (Day, 2000; Shtein *et al.*, 2016). When the exocarp is dehydrated, because of the resistance of the sclerenchyma cells in the vascular bundle, the pericarp can only produce very slight deformation even if the parenchyma cells around the vascular bundle contract greatly due to water loss, and thus the exocarp is not able to open independently. When the exocarp is fully opened by external force, it produces a large passive deformation, which leads to a significant change in the surface curvature. The water drop-like shape of the indehiscent exocarp causes the opening of the exocarp to be similar to the opening process of the insect-trapping leaves of some carnivorous plants (Forterre *et al.*, 2005; Westermeier *et al.*, 2018). During these movement processes, a large amount of energy is required to overcome geometric constraints (Audoly and Pomeau, 2010; Forterre, 2013). Fracturing of the boundary line of the basal flat area before the seed is released destroys the continuity of the exocarp surface, simplifying the opening process of the exocarp. Although the fracture process consumes some stored energy, the thinness and particular shape of the basal flat area of *O. japonica* may minimize energy consumption similar to the fruit dehiscence in *Impatiens glandulifera* (Deegan, 2012).

Unlike the exocarp, the endocarp of *O. japonica* undergoes clear deformation movement during dehydration, known as hygroscopic movement. In mature fruits, the endocarp cells are all dead with thickened cell walls, which form a typical sandwich structure. The core porous part of this structure is the hygroscopically active element, and the two sheet parts are the resistance elements in different directions. Such configurations have been found in the capsule of sesame, but the two resistance layers of sesame are adjacent to each other and lie on the inner side of the capsule rather than being separated on either side of the active layer (Shtein *et al.*, 2016). After the sesame capsule dehydrates, it bends outward simultaneously in longitudinal and transverse directions. In contrast, the endocarp of *O. japonica* tends to bend in the opposite direction at a certain angle, which produces a geometric incompatibility (Efrati *et al.*, 2009). The initial flat pods of some leguminous plants having a geometric incompatibility tend to form two helical strips in opposite directions during fruit dehiscence (Armon *et al.*, 2011). Although the endocarp of *O. japonica* is not flat but water drop-shaped before opening, the presence of a ventral opening makes it appear as a curved plate in shape. After opening, the two sides of the endocarp of *O. japonica* also show chiral bending configurations, but on the same side of the endocarp there are also two bending areas in the opposite directions that occur in different parts of the endocarp. This particular deformation makes the initially water drop-shaped endocarp become open arm-shaped after fruit dehiscence.

There are clear differences in the deformation of the exocarp and endocarp during fruit dehiscence, and they play different roles in the explosive seed dispersal of *O. japonica*. The endocarp provides power for seed launch through dehydration, while the exocarp resists the opening of the endocarp and provides other additional functions. The pericarp opens very slowly during the explosive seed dispersal of *O. japonica*, and seed launch takes place only at the last stage of the opening. This process is different from that of explosive seed dispersal in other plants, in which pericarp opening is generally fast, and seed launching occurs simultaneously with opening of the pericarp (Witztum and Schulgasser, 1995; Hayashi *et al.*, 2009; Vaughn *et al.*, 2011). Before the seed of *O. japonica* leaves the fruit, the split of the exocarp driven by the endocarp is crucial for seed launch. The top opening formed by the opening of the exocarp provides a passage for separation of the seed, whereas the ventral edge of the exocarp provides an acceleration slide for detachment of the endocarp from the exocarp. When the arm-shaped endocarp rapidly slides out of the exocarp, the seed is accelerated to launch speed in a very short time by the endocarp. The kinetic energy of seed and endocarp flight is derived from the elastic potential energy released by the endocarp, which has accumulated as a result of exocarp resistance to the deformation movement of the endocarp. The relatively low weight and large elastic modulus of the endocarp ensure that the seed and endocarp can obtain relatively high initial velocity when they are separated from the exocarp (Vogel, 2005). However, the shape of the endocarp is not conducive to its high-speed flight with the seed in the air, and therefore the seed needs to be quickly separated from the endocarp to ensure that it can be dispersed as far as possible. This process is accomplished by squeezing the ovary area of the opening endocarp to the seed, although this squeezing does not directly provide energy for launch of the seed. The mechanisms of movement of the pericarp and acceleration of seed launch mean the two layers of pericarp form a structure similar to a unique slingshot, which can launch the seed from the fruit in the form of a bullet.

Launching is often the means for seed or spore dispersal in various plants (Edwards *et al.*, 2005; Noblin *et al.*, 2012; Sakes *et al.*, 2016). These launch processes are generally driven by the elastic potential energy accumulated in the reproductive organs through slow water movement between tissues (Dumais and Forterre, 2012). Based on the method of energy transition, the launch mechanisms in plants can be divided into three categories: pressure launch, coiling launch and squeeze launch. The latter two occur in the largest number of species, and are based on the deformation of reproductive organs (Sakes *et al.*, 2016). The reproductive organs that use coiling launch usually have long band- or long rod-shaped deformation structures, which are much larger than the size of the launch object, such as the long rod-shaped filaments in explosive pollen release and the long band-shaped peel valves in explosive seed dispersal (Van der Burgt, 1997; Whitaker *et al.*, 2007; Nimmo *et al.*, 2014; Hofhuis *et al.*, 2016; Galstyan and Hay, 2018). During explosive dispersal processes, pollen grains and seeds are accelerated directly with the deformation movement of these structures. Plants that spread seeds autonomously by the squeeze launch mechanism usually have various pericarp shapes with sizes similar to that of the seed (Swaine and Beer, 1977; Roberts and Haynes, 1983). The pericarp of these plants completes the launch process by squeezing the seeds directly outward through the deformation movement after the fruit ripens (Lisci and Pacini, 1997; Sakes *et al.*, 2016). *Orixa japonica* has a water drop-shaped peel which is only slightly larger than the seed. These morphological characteristics indicate that the fruit of *O. japonica* is not suitable for the coiling mechanism, whereas they are indicative of the squeeze launch mechanism. However, in the explosive seed dispersal of *O. japonica*, the seed is not squeezed by the peel, but accelerated by the interaction between the exocarp and endocarp, which depends on the hygroscopic coiling movement of the endocarp. This mechanism is based on the unique shape of the pericarp of *O. japonica* as well as the multi-layered internal structure.

In our observations of seed dispersal of *O. japonica*, a small proportion of the seeds (2/35) could not be separated from the endocarp and hence dispersed with the endocarp after seed launching. Seed dispersal with the endocarp is common in some autochorous plants of Rutaceae, such as *Metrodorea*, *Esenbeckia* and *Pilocarpus* (Souza *et al.*, 2005, 2008). In these plants, the lignified endocarp, as a resistance structure, participates in the squeeze launching process of seeds. At the same time, the stiff endocarp may also protect the internal seeds from some predators after seed dispersal. Although the endocarp and seed of *O. japonica* together can only be spread to the area close to the parent due to the high air resistance of the endocarp, similar to the Rutaceae plants mentioned above, the endocarp may provide protection for the internal seeds after seed dispersal, and the dry unfolded endocarp may help the inner seed to spread across distant areas due to strong winds.

SUPPLEMENTARY DATA

Supplementary data are available online at https://academic.oup.com/aob and consist of the following. Video S1: High-speed video (recording at 10 000 fps and playing at 15 fps) of the seed launch process from the abdomen of the fruit of *Orixa japonica* on a white cushion. Video S2: High-speed video (recording at 1000 fps and playing at 8 fps) of the seed launch process from the side of the fruit of *O. japonica* fixed on a small platform.

ACKNOWLEDGEMENTS

We thank Prof. Xiao-Fan Wang and Shi-Rui Gan for help with collection and cultivation. We thank Wen-Xuan Zhou for technical assistance. We also thank Shuai Wang for helpful suggestions on the manuscript. Thanks to the reviewers and editor for suggestions that improved the manuscript. The authors declare no competing interests.

FUNDING

This work was funded by a grant from the National Natural Science Foundation of China (NSFC 31600186).

LITERATURE CITED

Armon S, Efrati E, Kupferman R, Sharon E. 2011. Geometry and mechanics in the opening of chiral seed pods. *Science (New York, N.Y.)* **333**: 1726–1730.

Audoly B, Pomeau Y. 2010. *Elasticity and geometry: from hair curl to the nonlinear behavior of shells.* Oxford: Oxford University Press.

Bar-On B, Sui X, Livanov K, *et al.* 2014. Structural origins of morphing in plant tissues. *Applied Physics Letters* **105**: 033703.

Chen PY, McKittrick J, Meyers MA. 2012. Biological materials: Functional adaptations and bioinspired designs. *Progress in Materials Science* **57**: 1492–1704.

Day JS. 2000. Anatomy of capsule dehiscence in sesame varieties. *The Journal of Agricultural Science* **134**: 45–53.

Deegan RD. 2012. Finessing the fracture energy barrier in ballistic seed dispersal. *Proceedings of the National Academy of Sciences of the United States of America* **109**: 5166–5169.

Dumais J, Forterre Y. 2012. "Vegetable Dynamicks": the role of water in plant movements. *Annual Review of Fluid Mechanics* **44**: 453–478.

Edwards J, Whitaker D, Klionsky S, Laskowski MJ. 2005. Botany: a record-breaking pollen catapult. *Nature* **435**: 164.

Efrati E, Sharon E, Kupferman R. 2009. Elastic theory of unconstrained non-Euclidean plates. *Journal of the Mechanics and Physics of Solids* **57**:762–775.

Elbaum R, Abraham Y. 2014. Insights into the microstructures of hygroscopic movement in plant seed dispersal. *Plant Science: An International Journal of Experimental Plant Biology* **223**: 124–133.

Endo Y, Sakamoto J, Kashiwano Y, Yokota H, Nakamura S, Kinoshita E. 2010. A biomechanical study on burst mechanisms of plant fruit: stress analysis of pericarps before bursting. *Journal of the Mechanical Behavior of Biomedical Materials* **3**: 512–519.

Evangelista D, Hotton S, Dumais J. 2011. The mechanics of explosive dispersal and self-burial in the seeds of the filaree, *Erodium cicutarium* (Geraniaceae). *The Journal of Experimental Biology* **214**: 521–529.

Forterre Y. 2013. Slow, fast and furious: understanding the physics of plant movements. *Journal of Experimental Botany* **64**: 4745–4760.

Forterre Y, Skotheim JM, Dumais J, Mahadevan L. 2005. How the venus flytrap snaps. *Nature* **433**: 421–425.

Funayama S, Murata K, Nozoe S. 1994. Quinoline alkaloids from *Orixa japonica*. *Phytochemistry* **36**: 525–528.

Galstyan A, Hay A. 2018. Snap, crack and pop of explosive fruit. *Current Opinion in Genetics & Development* **51**: 31–36.

Hayashi M, Feilich KL, Ellerby DJ. 2009. The mechanics of explosive seed dispersal in orange jewelweed (*Impatiens capensis*). *Journal of Experimental Botany* **60**: 2045–2053.

Hofhuis H, Hay A. 2017. Explosive seed dispersal. *The New Phytologist* **216**: 339–342.

Hofhuis H, Moulton D, Lessinnes T, *et al.* 2016. Morphomechanical innovation drives explosive seed dispersal. *Cell* **166**: 222–233.

Howe HF, Smallwood J. 1982. Ecology of seed dispersal. *Annual Review of Ecology and Systematics* **13**: 201–228.

Lisci M, Pacini E. 1997. Fruit and seed structural characteristics and seed dispersal in *Mercurialis annua* L. (Euphorbiaceae). *Acta Societatis Botanicorum Poloniae* **66**: 379–386.

Nimmo JR, Hermann PM, Kirkham MB, Landa ER. 2014. Pollen dispersal by catapult: experiments of Lyman J. Briggs on the flower of Mountain Laurel. *Physics in Perspective* **16**: 371–389.

Noblin X, Rojas NO, Westbrook J, Llorens C, Argentina M, Dumais J. 2012. The fern sporangium: a unique catapult. *Science (New York, N.Y.)* **335**: 1322.

Roberts ML, Haynes RR. 1983. Ballistic seed dispersal in *Illicium* (Illiciaceae). *Plant Systematics and Evolution* **143**: 227–232.

Sakes A, van der Wiel M, Henselmans PW, van Leeuwen JL, Dodou D, Breedveld P. 2016. Shooting mechanisms in nature: a systematic review. *PLoS One* **11**: e0158277.

Shtein I, Elbaum R, Bar-On B. 2016. The hygroscopic opening of sesame fruits is induced by a functionally graded pericarp architecture. *Frontiers in Plant Science* **7**: 1501.

Souza A, Mourão KSM, Souza LA. 2005. Morphology and anatomy of the fruit and seed in development of *Pilocarpus pennatifolius* Lem. (Rutaceae). *Revista Brasileria de Botnica* **28**: 745–754.

Souza LA, Rosa SM, Moscheta IS. 2008. Anatomy of the developing fruit of *Metrodorea nigra* A. St.-Hil. (Rutaceae). *Brazilian Archives of Biology and Technology* **51**:1171–1179.

Stamp NE, Lucas JR. 1983. Ecological correlates of explosive seed dispersal. *Oecologia* **59**: 272–278.

Swaine MD, Beer T. 1977. Explosive seed dispersal in *Hura crepitans* L. (Euphorbiaceae). *New Phytologist* **78**: 695–708.

Van der Burgt XM. 1997. Explosive seed dispersal of the rainforest tree *Tetraberlinia moreliana* (Leguminosae-Caesalpinioideae) in Gabon. *Journal of Tropical Ecology* **13**: 145–151.

Vaughn KC, Bowling AJ, Ruel KJ. 2011. The mechanism for explosive seed dispersal in *Cardamine hirsuta* (Brassicaceae). *American Journal of Botany* **98**: 1276–1285.

Vogel S. 2005. Living in a physical world II. The bio-ballistics of small projectiles. *Journal of Biosciences* **30**: 167–175.

Westermeier AS, Sachse R, Poppinga S, *et al.* 2018. How the carnivorous waterwheel plant (*Aldrovanda vesiculosa*) snaps. *Proceedings of the Royal Society B: Biological Sciences* **285**: 20180012.

Whitaker DL, Webster LA, Edwards J. 2007. The biomechanics of *Cornus canadensis* stamens are ideal for catapulting pollen vertically. *Functional Ecology* **21**: 219–225.

Witztum A, Schulgasser K. 1995. The mechanics of seed expulsion in Acanthaceae. *Journal of theoretical Biology* **176**: 531–542.

Zhang DX, Hartley TG. 2008. Orixa. In: Wu ZY, Raven PH. eds. *Flora of China,* Vol. **11**. Beijing; St. Louis: Science Press; Missouri Botanical Garden Press, 66.

Zohary AFM. 1955. On the pericarpial structure of the legume, its evolution and relation to dehiscence. *Phytomorphology* **5**: 99–111.